JACS
JOURNAL OF THE AMERICAN CHEMICAL SOCIETY

COMMUNICATION

pubs.acs.org/JACS

Pressure-Dependent Ion Current Rectification in Conical-Shaped Glass Nanopores

Wen-Jie Lan, Deric A. Holden, and Henry S. White*

Department of Chemistry, University of Utah, 315 South 1400 East, Salt Lake City, Utah 84112, United States

Supporting Information

ABSTRACT: Ion current rectification that occurs in conical-shaped glass nanopores in low ionic strength solutions is shown to be dependent on the rate of pressure-driven electrolyte flow through the nanopore, decreasing with increasing flow rate. The dependence of the $i-V$ response on pressure is due to the disruption of cation and anion distributions at equilibrium within the nanopore. Because the flow rate is proportional to the third power of the nanopore orifice radius, the pressure-driven flow can eliminate rectification in nanopores with radii of ~200 nm but has a negligible influence on rectification in a smaller nanopore with a radius of ~30 nm. The experimental results are in qualitative agreement with predictions based on finite-element simulations used to solve simultaneously the Nernst−Planck, Poisson, and Navier−Stokes equations for ion fluxes in a moving electrolyte within a conical nanopore.

Mass transfer through charged nanopores and nanochannels with asymmetric geometries has attracted significant attention during the past decade.[1−3] An interesting characteristic associated with charged conical nanopores is ion current rectification (ICR). ICR is defined as the asymmetric $i-V$ response of the nanopores, i.e., the departure from ohmic behavior.[4−8] ICR in a conical-shaped nanopore may arise from surface charges on the pore wall and the voltage-dependent depletion and accumulation of electrolyte ions near the nanopore orifice.[9] For negatively charged glass nanopores, the magnitude of the current through the nanopore at a negative potential (pore interior vs external solution) is larger than the current at a positive potential with the same magnitude.

We have been interested in the fabrication and analytical applications of glass and fused quartz nanopore membranes[10] (GNMs and QNMs, respectively) as nano-Coulter counters of particles and as lipid bilayer supports for ion channel recordings.[11] These conical-shaped nanopores can be prepared with orifice radii as small as a few nanometers, and they exhibit ICR behavior that is dependent on the ion concentration and nanopore radius.[12] Here we describe the dependence of the ICR behavior of conical-shaped GNMs on the pressure applied across the nanopore, as depicted in Scheme 1. We demonstrate that pressure-driven flow through the nanopore results in a decrease in ICR due to disruption of the equilibrium cation and anion distributions. The pressure-dependent ICR response is shown to be strongly dependent on the pore orifice size, in agreement with finite-element simulations presented below.

Scheme 1. Ion Distributions around the Orifice of the Negatively Charged Glass Nanopore Membrane (GNM) at Positive/Negative Potentials in the Absence and Presence of Pressure-Driven Flow[a]

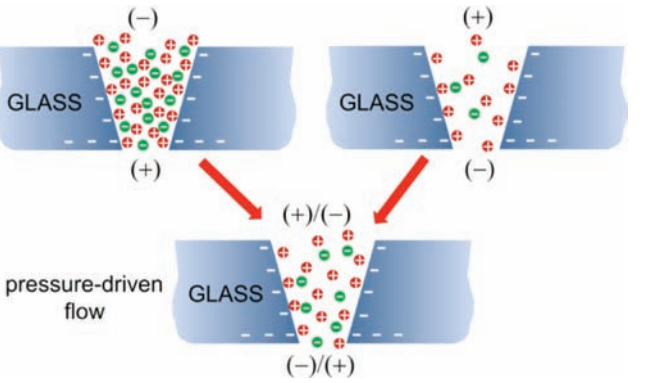

[a] If the flow is sufficiently large, the concentrations of both cations and anions in the nanopore are equal to the values in the bulk solution in contact with the nanopore. The + and − signs refer to the polarity of the voltage applied across the membrane.

GNMs containing a single conical-shaped nanopore in a glass membrane at the end of a glass capillary were prepared as previously described [see the Supporting Information (SI)]. The radii of the small orifices were determined by measuring the nanopore resistance in a 1 M KCl solution. The GNMs were rinsed with water and then filled with and immersed in a 0.01 M KCl solution (pH 7.3). Pressure was applied across the membrane using a syringe connected to the glass capillary containing the GNM (see the SI). The signs of both pressure and potential are defined as the value inside the nanopore relative to the value in the external solution.

Figure 1 shows the $i-V$ responses for nanopores with radii of 185 and 30 nm at pressures ranging from −160 to 160 mmHg (all radii herein refer to the dimension of the small orifice of the nanopore). In the absence of pressure, both nanopores displayed a significant nonlinear $i-V$ response, similar to previous reports.[9] Several models have been proposed to account for the phenomena of ICR. Here we use the ion depletion and accumulation model to qualitatively explain the ICR. Since the nanopore surface is negatively charged at neutral pH and the radius of the pore orifice is small, the region at the pore opening is cation-selective. At negative potentials, the K^+ flux is directed from the

Received: June 21, 2011
Published: July 29, 2011

dx.doi.org/10.1021/ja205773a | J. Am. Chem. Soc. 2011, 133, 13300–13303

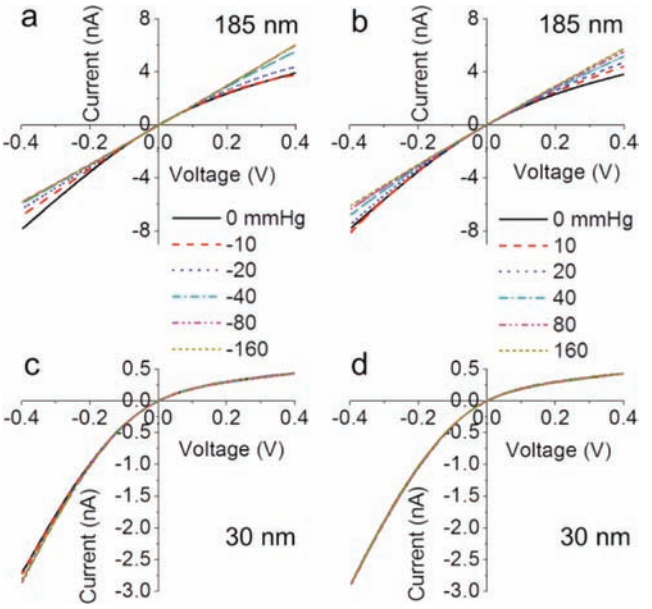

Figure 1. Pressure-dependent $i-V$ responses of conical-shaped GNMs with radii of (a, b) 185 and (c, d) 30 nm in a 0.01 M KCl solution containing 0.1 mM PBS buffer (pH 7.3). The scan rates were 30 and 50 mV/s for the 185 and 30 nm radius nanopores, respectively. The $i-V$ curves in the left column correspond to negative applied pressures and those in the right column to positive pressures (pore interior vs external solution).

external bulk solution to the pore interior while Cl^- moves in the opposite direction. As the pore is cation-selective, Cl^- ions are rejected by the glass surface because of electrostatic repulsion. A consequence of anion rejection is an increase in the K^+ and Cl^- concentrations within the pore interior, resulting in a nanopore conductivity greater than that based on the KCl concentration in the bulk solution. Conversely, when a positive potential relative to the external solution is applied inside the pore, the transport of Cl^- from the external solution to the internal solution is rejected by the surface charges, depleting Cl^- within the pore interior and thus decreasing the nanopore conductivity and the observed ionic current.[13,14] A larger conical-shaped nanopore displays a weaker rectification than a smaller pore because of the smaller extent of the ion electrical double layer into the pore. The above explanation is quantitatively supported by previous finite-element simulations in which the ion depletion and accumulation were observed by solving the Nernst−Planck and Poisson equations simultaneously.[15]

The 185 and 30 nm radius nanopores displayed qualitatively different ICR behaviors when negative or positive pressure was applied across the GNM. As shown in Figure 1a,b, an applied pressure across the larger pore (185 nm) resulted in a more ohmic $i-V$ response. The rectification factor, defined as the ratio of the ion current magnitude at −0.4 V to that at +0.4 V, decreased from ∼2 to ∼1 as the pressure increased from 0 to ±160 mmHg. Application of negative pressures reduced the ICR slightly more effectively than positive pressures, as shown in Figure 2a for positive and negative pressures between 0 and 160 mmHg. The dependence of the rectification factor on pressure was reversible, as shown in Figure 2b for pressure cycling between 0 and ±80 mmHg. In contrast, applied pressure had negligible effect on the more highly rectified $i-V$ response of the smaller pore (30 nm, Figure 1c,d). The rectification ratio was ∼6.6 at all pressures. In general, we observed a

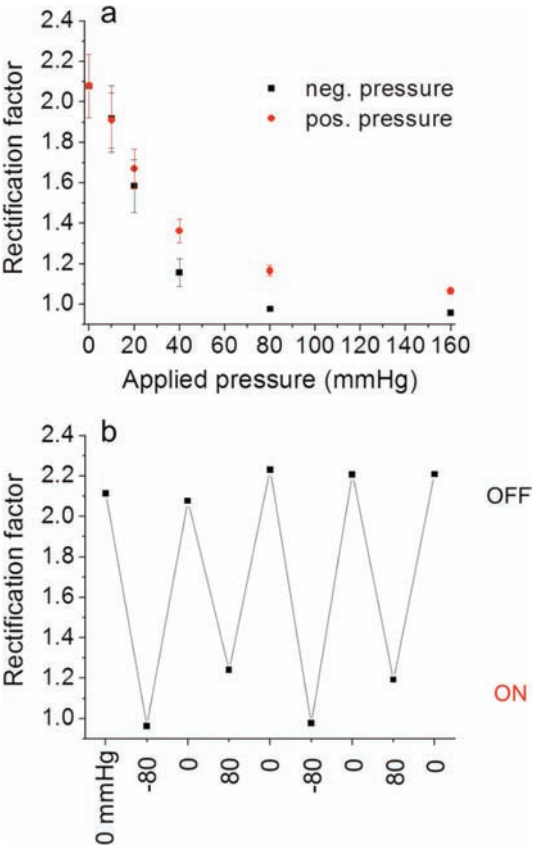

Figure 2. (a) Rectification factor as a function of applied pressure for a conical-shaped nanopore with a radius of 185 nm in a 0.01 M KCl solution (pH 7.3). (b) Rectification factor during pressure cycling between 0 and ±80 mmHg. The "OFF" and "ON" labels refer to the rectification factor in the absence and presence of the applied pressure.

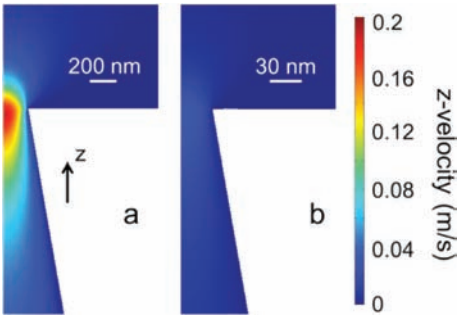

Figure 3. Simulated z velocity distributions (two-dimensional axial) for nanopores with radii of (a) 185 and (b) 30 nm at an applied pressure of 80 mmHg.

significant pressure dependence of the ICR for nanopores with radii of ∼180 nm or larger.

The pressure-dependent ICR behavior can be readily understood in terms of the effect of flow on the ion distributions near the nanopore orifice. The applied pressure across the GNM engenders a volumetric flow Q through the conical-shaped nanopore estimated by $Q = 3\pi r^3 \Delta P/(8\eta \cot \theta)$, where r is the radius of the pore orifice, ΔP is the pressure difference across the nanopore, η is the solution viscosity, and θ is the half-cone angle of the nanopore.[16] Q is proportional to r^3 at constant ΔP.

dx.doi.org/10.1021/ja205773a |J. Am. Chem. Soc. 2011, 133, 13300–13303

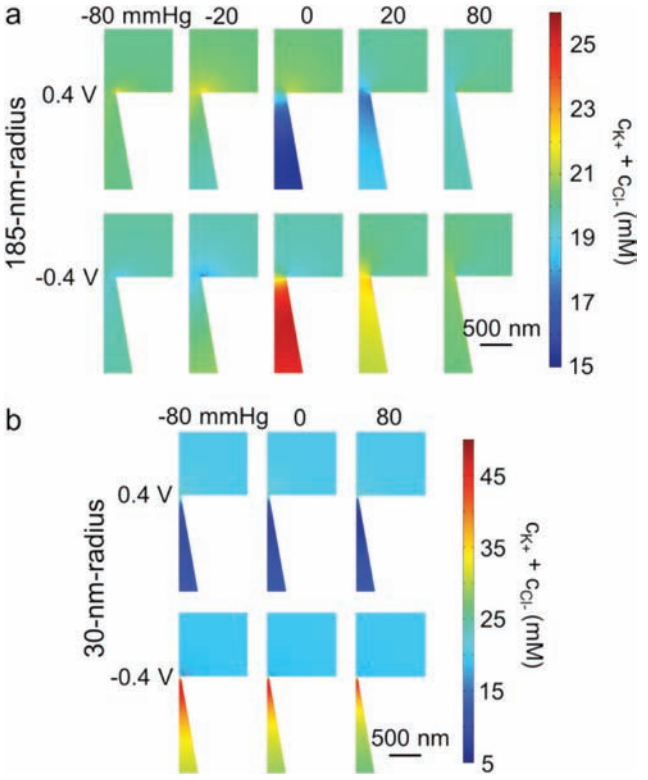

Figure 4. Simulated distributions of the total ion concentration (K^+ and Cl^-) near the orifice for GNMs with radii of (a) 185 and (b) 30 nm as functions of applied potential and pressure (both pore interior vs external solution) in 0.01 M KCl solution.

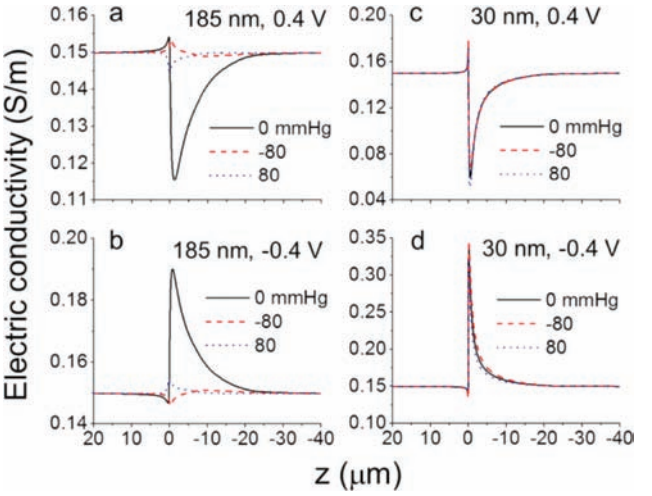

Figure 5. Simulated electric conductivity distributions for pores with radii of (a, b) 185 and (c, d) 30 nm as functions of distance along the central pore axis under different pressures at (a, c) 0.4 and (b, d) −0.4 V (pore interior vs external solution). The opening of the pore is located at $z = 0$ μm in each figure; $z < 0$ μm corresponds to the nanopore interior and $z > 0$ μm to the external solution.

Thus, the volumetric rate is greater by a factor of ~235 for the 185 nm radius GNM than for the 30 nm radius GNM. The flow brings solution containing bulk concentrations of K^+ and Cl^- ions (0.01 M) into the nanopore, disrupting the equilibrium ion concentrations induced by the charged glass surface. Finite-element simulations employing the Navier−Stokes equation to compute the fluid velocity distributions near the pore orifice (Figure 3) demonstrated that an applied pressure of 80 mmHg creates a large velocity gradient near the orifice of a 185 nm radius pore but has a relatively negligible effect on the flow through a 30 nm radius pore. These results indicate that an applied pressure should result in qualitatively different ICR dependences for large and small nanopores, in agreement with the data shown in Figure 1. Qualitatively, the different dependences of Q and the ion distributions on the pore size result in different pressure-dependent ICR behaviors as a function of nanopore size.

In order to better understand the pressure- and size-dependent $i-V$ behaviors, finite-element computations were performed to solve simultaneously the Nernst−Planck equation for the ion fluxes, the Poisson equation relating the ion concentrations to the local electric field, and the Navier−Stokes equation for solution flow. The simulations were similar to the ICR simulations published previously,[15] and details of the simulation boundary conditions and so on are presented in the SI.

Figure 4a shows distributions of the total ion concentration (K^+ and Cl^-) near the pore orifice at different potentials and pressures for a 185 nm radius GNM. In the absence of an applied pressure (0 mmHg, middle column), the depletion of ions in the pore interior at positive potential and the accumulation of the ions at negative potential are apparent, and they result in significant ICR as previously described. Upon application of a pressure, the induced flow brings in solution containing K^+ and Cl^- ions at their bulk concentrations (0.01 M), removing the depletion or excess of ions responsible for ICR. Thus, the total concentration at the orifice is closer to that of the bulk solution, resulting in a more ohmic behavior in agreement with the experimental observations. The simulations also indicated that for the 185 nm radius pore, negative pressures are slightly more effective in producing a uniform concentration distribution within the pore. A consequence of the asymmetry in the pressure dependence is that negative pressures are more effective than positive pressures in producing an ohmic $i-V$ response, as shown in Figure 2.

The finite-element simulations of the total ion concentration for the 30 nm radius pore (Figure 4b) also demonstrated that an applied pressure has negligible effect on ICR for this pore. Although larger ion depletion/accumulation effects and thus a more pronounced rectified $i-V$ response are associated with the smaller nanopore, the greatly reduced rate of flow through the smaller nanopore results in an insignificant pressure dependence of the ICR.

Figure 5a,b shows solution conductivity profiles along the central nanopore axis ($r = 0$) at different pressures and potentials for a 185 nm radius pore. The conductivity in the pore decreases at the positive potential and increases at the negative potential relative to the value of the bulk 0.01 M KCl solution (0.15 S/m) in contact with the nanopore on both sides, consistent with the qualitative explanation of ICR presented above and reported previously.[15] When a negative or positive pressure (80 mmHg in magnitude) is applied across the pore, the gradient in the electric conductivity nearly vanishes. The flat conductivity profiles at 80 and −80 mmHg correspond more closely to that for an uncharged nanopore, in which no ion depletion or accumulation is expected (or observed in finite-element simulations). The simulations in Figure 5 also demonstrate that the direction of the applied pressure across the GNM (+80 vs −80 mmHg) results in a small but significant difference in the nanopore conductivity at both positive and negative voltages. At the positive voltage,

application of 80 mmHg nearly restores the nanopore conductivity to the bulk-solution value (Figure 5a), but a small residual *decrease* in conductivity is observed around the pore orifice ($z = 0$). Conversely, at −80 mmHg, a small residual *increase* in conductivity is observed. The difference between the residuals at negative and positive pressures may be responsible for the small difference in the experimental $i-V$ curves at ±80 mmHg. In contrast, the conductivity profiles for a 30 nm radius pore (Figure 5c,d) are nearly independent of the applied pressure, consistent with the applied pressure having a negligible effect on the $i-V$ response (Figure 1).

Simulations of the full pressure-dependent $i-V$ curves for nanopores with radii of 185 and 30 nm are presented in the SI. While the finite-element simulations successfully predict all of the qualitative trends of the pressure-dependent rectification, they fail to predict rectification factors that quantitatively match the experimental observations at different applied pressures. Both our experiments and simulations suggest that overlap of the electrical double layer is apparently not required to achieve significant ICR, in agreement with phenomena reported previously by Jacobson,[17] Wang,[18] and our group.[12] For a 0.01 M KCl solution as employed here, the electrical double layer associated with the glass surface charge is ∼15 nm (5 times the Debye length) and thus extends only a fraction of the distance into the interior of the 185 nm radius nanopore. It is also worthwhile to mention that the currents at negative potentials under small positive pressures were sometimes slightly larger than the currents in the absence of pressure (e.g., compare the red dashed line for 10 mmHg and the black solid line at 0 mmHg in Figure 1b). However, this phenomenon was not reproducibly observed for all GNMs of similar size (Figure SI5). The origin of this second-order effect is not understood; we speculate that flow at low pressure results in a small compression of the ion concentration gradients at the pore orifice, producing a slightly higher conductivity at negative potentials.

In summary, we have reported a previously unobserved but fundamental aspect of the relationship between fluid flow and ion fluxes in an electrically charged nanopore. The ion redistributions around the nanopore orifice are determined by a combination of the electrostatic forces associated with the surface charge and finite solution conductivity and by the volumetric flow induced by the pressure. Finite-element simulations of the electric field, ion concentration, and flow rate have provided insight into the origin of the pressure-dependent ICR and are in semiquantitative agreement with the experimental observations.

■ ASSOCIATED CONTENT

Ⓢ Supporting Information. Experimental details, estimation of glass nanopore membrane surface charge, finite-element simulation details, and pressure-dependent $i-V$ curves for a 207 nm radius pore. This material is available free of charge via the Internet at http://pubs.acs.org.

■ AUTHOR INFORMATION

Corresponding Author
white@chem.utah.edu

■ ACKNOWLEDGMENT

Support from the National Science Foundation and the Defense Advanced Research Project Agency is gratefully acknowledged. W.J.L. thanks Mr. C. Kubeil (Technische Universität Dresden, Germany) and Mr. P. Yang (University of Utah) for helpful discussions.

■ REFERENCES

(1) Wei, C.; Bard, A. J.; Feldberg, S. W. *Anal. Chem.* **1997**, *69*, 4627.
(2) (a) Jin, P.; Mukaibo, H.; Horne, L. P.; Bishop, G. W.; Martin, C. R. *J. Am. Chem. Soc.* **2010**, *132*, 2118. (b) Sexton, L. T.; Mukaibo, H.; Katira, P.; Hess, H.; Sherrill, S. A.; Horne, L. P.; Martin, C. R. *J. Am. Chem. Soc.* **2010**, *132*, 6755. (c) Sexton, L. T.; Horne, L. P.; Sherrill, S. A.; Bishop, G. W.; Baker, L. A.; Martin, C. R. *J. Am. Chem. Soc.* **2007**, *129*, 13144. (d) Siwy, Z.; Trofin, L.; Kohli, P.; Baker, L. A.; Trautmann, C.; Martin, C. R. *J. Am. Chem. Soc.* **2005**, *127*, 5000.
(3) (a) Yusko, E. C.; An, R.; Mayer, M. *ACS Nano* **2010**, *4*, 477. (b) Han, J. H.; Kim, K. B.; Kim, H. C.; Chung, T. D. *Angew. Chem., Int. Ed.* **2009**, *48*, 3830. (c) Umehara, S.; Pourmand, N.; Webb, C. D.; Davis, R. W.; Yasuda, K.; Karhanek, M. *Nano Lett.* **2006**, *6*, 2486.
(4) (a) Vlassiouk, I.; Kozel, T. R.; Siwy, Z. S. *J. Am. Chem. Soc.* **2009**, *131*, 8211. (b) He, Y.; Gillespie, D.; Boda, D.; Vlassiouk, I.; Eisenberg, R. S.; Siwy, Z. S. *J. Am. Chem. Soc.* **2009**, *131*, 5194. (c) Siwy, Z.; Heins, E.; Harrell, C. C.; Kohli, P.; Martin, C. R. *J. Am. Chem. Soc.* **2004**, *126*, 10850. (d) Vlassiouk, I.; Siwy, Z. S. *Nano Lett.* **2007**, *7*, 552.
(5) (a) Yameen, B.; Ali, M.; Neumann, R.; Ensinger, W.; Knoll, W.; Azzaroni, O. *J. Am. Chem. Soc.* **2009**, *131*, 2070. (b) Ali, M.; Yameen, B.; Cervera, J.; Ramirez, P.; Neumann, R.; Ensinger, W.; Knoll, W.; Azzaroni, O. *J. Am. Chem. Soc.* **2010**, *132*, 8338. (c) Ali, M.; Nguyen, Q. H.; Neumann, R.; Ensinger, W. *Chem. Commun.* **2010**, *46*, 6690.
(6) (a) Hou, X.; Yang, F.; Li, L.; Song, Y.; Jiang, L.; Zhu, D. *J. Am. Chem. Soc.* **2010**, *132*, 11736. (b) Xia, F.; Guo, W.; Mao, Y.; Hou, X.; Xue, J.; Xia, H.; Wang, L.; Song, Y.; Ji, H.; Ouyang, Q.; Wang, Y.; Jiang, L. *J. Am. Chem. Soc.* **2008**, *130*, 8345. (c) Hou, X.; Dong, H.; Zhu, D.; Jiang, L. *Small* **2010**, *6*, 361.
(7) Guerrette, J. P.; Zhang, B. *J. Am. Chem. Soc.* **2010**, *132*, 17088.
(8) (a) Sa, N. Y.; Baker, L. A. *J. Am. Chem. Soc.* **2011**, *133*, 10398. (b) Sa, N. Y.; Fu, Y. Q.; Baker, L. A. *Anal. Chem.* **2010**, *82*, 9963.
(9) Siwy, Z. S. *Adv. Funct. Mater.* **2006**, *16*, 735.
(10) (a) Zhang, B.; Galusha, J.; Shiozawa, P. G.; Wang, G.; Bergren, A. J.; Jones, R. M.; White, R. J.; Ervin, E. N.; Cauley, C. C.; White, H. S. *Anal. Chem.* **2007**, *79*, 4778. (b) Schibel, A. E. P.; Edwards, T.; Kawano, R.; Lan, W. J.; White, H. S. *Anal. Chem.* **2010**, *82*, 7259.
(11) (a) Lan, W. J.; Holden, D. A.; Zhang, B.; White, H. S. *Anal. Chem.* **2011**, *83*, 3840. (b) White, R. J.; Ervin, E. N.; Yang, T.; Chen, X.; Daniel, S.; Cremer, P. S.; White, H. S. *J. Am. Chem. Soc.* **2007**, *129*, 11766. (c) Holden, D. A.; Hendrickson, G.; Lyon, L. A.; White, H. S. *J. Phys. Chem. C* **2011**, *115*, 2999.
(12) White, R. J.; Zhang, B.; Daniel, S.; Tang, J. M.; Ervin, E. N.; Cremer, P. S.; White, H. S. *Langmuir* **2006**, *22*, 10777.
(13) Woermann, D. *Phys. Chem. Chem. Phys.* **2003**, *5*, 1853.
(14) Cervera, J.; Schiedt, B.; Ramirez, P. *Europhys. Lett.* **2005**, *71*, 35.
(15) (a) White, H. S.; Bund, A. *Langmuir* **2008**, *24*, 2212. (b) Kubeil, C.; Bund, A. *J. Phys. Chem. C* **2011**, *115*, 7866. (c) Ai, Y.; Zhang, M.; Joo, S. W.; Cheney, M. A.; Qian, S. *J. Phys. Chem. C* **2010**, *114*, 3883.
(16) Lan, W. J.; Holden, D. A.; Liu, J.; White, H. S. *J. Phys. Chem. C*, **2011**, in press, doi: 10.1021/jp204839j.
(17) (a) Kovarik, M. L.; Zhou, K.; Jacobson, S. C. *J. Phys. Chem. B* **2009**, *113*, 15960. (b) Perry, J. M.; Zhou, K.; Harms, Z. D.; Jacobson, S. C. *ACS Nano* **2010**, *4*, 3897.
(18) Feng, J.; Liu, J.; Wu, B.; Wang, G. *Anal. Chem.* **2010**, *82*, 4520.